

## Extended scale invariance in the vortices of freely evolving two-dimensional turbulence

B. H. Burgess,<sup>\*</sup> D. G. Dritschel, and R. K. Scott

*School of Mathematics and Statistics, University of St Andrews, St Andrews KY16 9SS, United Kingdom*

(Received 6 March 2017; published 16 November 2017)

We report the existence of a self-similar scaling in the vortices of freely evolving two-dimensional turbulence: The vortex number density  $n(A,t)$  compensated by the mean vortex intensity  $\overline{\omega_v^2}(A,t)$ , where  $A$  is vortex area and  $t$  is time, follows the self-similar form  $n(A,t)/\overline{\omega_v^2}(A,t) \sim t^{-2/3} A^{-1}$ . This extended scale-invariant behavior holds for different initial conditions, despite very different scaling of  $n(A,t)$  and  $\overline{\omega_v^2}(A,t)$  taken separately, and ensures that the number of turnaround times  $[\overline{\omega_v^2}(A,t)]^{-1/2}$  taken to cross the characteristic intervortex distance is independent of scale.

DOI: [10.1103/PhysRevFluids.2.114702](https://doi.org/10.1103/PhysRevFluids.2.114702)

### I. INTRODUCTION

Two-dimensional turbulence is a paradigmatic model for the study of scaling far from equilibrium, with a broad range of applications to systems as diverse as large-scale geophysical and astrophysical fluid flows, black brane instabilities within the fluid-gravity correspondence [1], and trapped atomic gases [2]. Coherent vortices (localized, long-lived, rapidly rotating structures) form generically in both freely evolving and forced two-dimensional turbulence from extrema of the initial vorticity or forcing field, merging and generating a population distributed across scales and evolving in time [3–8]. In the freely evolving system, filaments thin exponentially fast, and at late times coherent vortices contain almost all the energy and dominate the flow evolution. An account of freely evolving turbulence in the long time limit therefore amounts to a theory for the vortex population.

Several increasingly complex scaling theories have been proposed to describe vortices in freely evolving two-dimensional turbulence. Considering only spatial scaling, Refs. [3,4] linked the energy spectrum to an algebraic distribution of vortex areas  $n(A) \sim A^{-p}$ , where  $n(A)$  is the number density of vortices with area  $A$  and  $p$  was measured from numerical simulations. Separately, Refs. [5,6] developed a temporal scaling theory for a dilute gas of  $N$  identical vortices with density  $\rho \sim t^\xi$ . Subsequently, a number of theoretical predictions for the scaling exponent  $\xi$  were made [9–16], with values ranging from  $\xi = 2/3$  [13] to  $\xi = 1$  [9,11,12,15].

The first combined spatiotemporal theory for the vortex population was developed in [7]. The theory assumes that vortices with a range of areas  $A$  and uniform intensities contain most of the energy in the system and that the vortex area distribution is scale invariant  $n(A,t) = c(t)A^{-1}$ , where  $c(t)$  is dimensionless. Here the vortex intensity is defined as the mean square vorticity evaluated over vortices of area  $A$ ,

$$\overline{\omega_v^2}(A,t) \equiv \frac{1}{N} \sum_{i=1}^N \frac{1}{A_i} \int_{A_i} \omega^2 dx dy, \quad (1)$$

where the overline on  $\overline{\omega_v^2}(A,t)$  denotes an average over vortex areas  $A_i$  in a bin centered on  $A$ ,  $A_i \in [A - dA, A + dA]$ , and  $N$  is the total number of such vortices. In [7] it was assumed that the vortex intensity was constant as a function of both vortex area  $A$  and time  $t$ , i.e., that  $\overline{\omega_v^2}(A,t) \equiv \overline{\omega_v^2} = \text{const}$ . In the present study we will consider the more general case in which  $\overline{\omega_v^2}(A,t)$

---

<sup>\*</sup>bhb3@st-andrews.ac.uk

varies with both  $A$  and  $t$  and explore the implications for the scaling properties of the vortex number density  $n(A, t)$ .

Under the assumption that vortex self-energies dominate the kinetic energy, Ref. [7] identified the vortex energy

$$E_v = \frac{1}{2\mathcal{D}} \int_{A_{\min}}^{A_{\max}} \frac{1}{\omega_v^2} A^2 n(A, t) dA \sim c(t) A_{\max}^2 \quad (2)$$

with the total kinetic energy

$$E = \frac{1}{2\mathcal{D}} \int |\mathbf{u}|^2 dx dy \quad (3)$$

such that  $E \sim E_v$ . Here  $\mathcal{D}$  is the area of a finite region large enough that the statistics converge and  $\mathbf{u}$  is the fluid velocity. The integration limits in (2) are  $A_{\max}(t)$ , the area of the largest vortex, and  $A_{\min}$ , a minimum allowed vortex area, which is fixed and chosen larger than the smallest resolved area. Energy  $E \sim E_v$  is conserved in freely evolving turbulence, which implies  $c(t) \sim A_{\max}^{-2}$ , where we have used Eq. (2).

Requiring the enstrophy to decay at the same rate at all scales, thereby preserving self-similarity, a differential equation can be derived (see [7]) for the area of the largest vortex, with the solution

$$A_{\max} \sim t^{1/3}. \quad (4)$$

Together with energy conservation, this yields  $c(t) \sim t^{-2/3}$ , so that

$$n(A, t) \sim t^{-2/3} A^{-1}. \quad (5)$$

The vortex enstrophy  $Z_v$  then decays as

$$Z_v = \frac{1}{2\mathcal{D}} \int_{A_{\min}}^{A_{\max}} \frac{1}{\omega_v^2} A n(A, t) dA \sim t^{-1/3}. \quad (6)$$

This global decay rate also holds locally in  $A$  space, consistent with the assumption of scale-invariant enstrophy decay: Specifically,  $Z_v \sim t^{-1/3}$  and  $E_v$  is conserved when the integral is over a comoving interval  $[\mu A_0(t), A_0(t)]$ , where  $0 < \mu < 1$  is a constant and  $A_0(t) \sim t^{1/3}$  grows like the largest vortex area. Note that  $\mu$  can take any value in  $(0, 1)$  as long as  $\mu A_0(t)$  and  $A_0(t)$  both fall within the scaling range of interest at all times considered. The comoving interval  $[\mu A_0(t), A_0(t)]$  represents a range of scales that grows along with the dilatation of flow features as measured by vortex growth through merger; hence, we are requiring invariance under the scaling transformation associated with the flow evolution. The notion of conservation in comoving intervals was inspired by the cosmological concept of a comoving frame, i.e., a reference frame dilating along with the expansion of the universe [17], and was applied in [8] to vortices in the forced inverse energy cascade to predict three scaling ranges conserving the first three moments of the number density.

We define a vortex area  $A$  as a region of intense vorticity enclosed by a vorticity isoline. This definition satisfies two widely accepted requirements, namely, that vortices are concentrated regions of intense vorticity and that they propagate with a high degree of material invariance [18]. The latter requirement is satisfied by selecting level sets of vorticity as vortex boundaries, since vorticity isolines are effectively frozen in at high Reynolds number. Our definition of a vortex area  $A$  is motivated by the desire to describe the flow in a way likely to yield new insights into turbulent dynamics: There are theoretical reasons to expect vorticity isolines and their enclosed areas to be especially significant in the description of two-dimensional turbulence. For example, the approach of contour dynamics relies on the fact that the equations of motion for an incompressible Eulerian fluid can be formulated in terms of vorticity isolines [19]. Furthermore, an action principle exists for two-dimensional incompressible fluids in which the canonical coordinates are isovorticity lines, with vorticity densities as the conjugate momenta [20]. The vortex identification method reflecting these theoretical considerations and our definition of a vortex area  $A$  is a threshold on vorticity.

TABLE I. Simulation parameters:  $N$  is the inversion grid resolution,  $N_{\text{eff}}$  is the effective resolution,  $s$  is the order of viscosity for the PS simulations,  $\nu$  is the viscosity,  $\mathcal{E}_0(k)$  is the form of the initial energy spectrum, with  $H$  the Heaviside step function, and  $\text{Re}(0)$  is the initial Reynolds number.

Run	$N^2$	$N_{\text{eff}}^2$	$s$	$\nu$	$\mathcal{E}_0(k)$	$\text{Re}(0)$
mGauss-CA	2048 <sup>2</sup>	32 768 <sup>2</sup>			$k^3 e^{-2(k/256)^2}$	$1.85 \times 10^4$
Tophat-CA	2048 <sup>2</sup>	32 768 <sup>2</sup>			$[H(k - 26.5) - H(k - 101.5)]$	$2.62 \times 10^5$
Gauss-PS	8192 <sup>2</sup>	3072 <sup>2</sup>	4	$1.26 \times 10^{-27}$	$e^{-2(k-512)^2/50^2}$	36
Tophat-PS	8192 <sup>2</sup>	3072 <sup>2</sup>	4	$1.26 \times 10^{-27}$	$[H(k - 212) - H(k - 812)]$	36

A key assumption in [7,8] is that the vortex intensity  $\overline{\omega_v^2}$  is constant in time and independent of vortex area  $A$ . Here we find that the distribution of  $\overline{\omega_v^2}(A,t)$  across scales is sensitive to the initial conditions in both contour advection and standard pseudospectral simulations of freely evolving two-dimensional turbulence. We consider two kinds of initial conditions: top-hat energy spectra constant over a range of wave numbers and initial spectra that are moments of Gaussian distributions in  $k$  space. The latter initial conditions yield vortex intensities  $\overline{\omega_v^2}(A,t)$  that are nonuniform in  $A$  and evolving in time. In these cases we show that an extended scale invariance in which

$$n(A,t)/\overline{\omega_v^2}(A,t) \sim t^{-2/3} A^{-1} \quad (7)$$

holds. More specifically,  $\overline{\omega_v^2}(A,t)$  and  $n(A,t)$  evolve to distributions that ensure that vortices cross the characteristic intervortex distance in the same number of turnaround times  $T_v(A,t) \equiv [\overline{\omega_v^2}(A,t)]^{-1/2}$  independent of scale, which is a basic requirement for self-similar dynamics. As we will see, the scaling  $n(A,t) \sim t^{-2/3} A^{-1}$  originally proposed in [7] is recovered for top-hat initial energy spectra, in which case  $\overline{\omega_v^2}(A,t)$  varies more weakly with  $A$  and  $t$ .

## II. METHODS

We use two numerical methods to study the scaling properties of the vortex intensity and number density. The first is contour advection (CA) performed by the combined Lagrangian advection method [21] on a 2048<sup>2</sup> basic inversion grid, with effective resolution  $N_{\text{eff}}^2 = (16 \times 2048)^2 = 32\,768^2$ . Contour surgery removes exceedingly thin filaments (here at  $1/32\,768$  the domain width), but preserves sharp vorticity gradients indefinitely. The simulation labeled mGauss-CA starts from an initial energy spectrum  $\mathcal{E}_0(k) \sim k^3 e^{-2(k/k_0)^2}$  with  $k_0 = 256$  on a 2048<sup>2</sup> inversion grid, while simulation Tophat-CA starts from a top-hat energy spectrum  $\mathcal{E}_0(k) \sim H(k - 26.5) - H(k - 101.5)$ , where  $H$  is the Heaviside step function, centered on  $k_0 = 64$  with  $\mathcal{E}_0(k)$  constant for  $k \in [26.5, 101.5]$  on a 2048<sup>2</sup> inversion grid.

Our second numerical approach is a standard pseudospectral (PS) method at resolution 8192<sup>2</sup> with fourth-order hyperviscosity. The pseudospectral simulation labeled Gauss-PS starts from a Gaussian initial energy spectrum  $\mathcal{E}(k) \sim e^{-(k-k_0)^2/\sigma^2}$ , with  $k_0 = 512$  and  $\sigma = 50$ , while the simulation labeled Tophat-PS starts from a top-hat energy spectrum  $\mathcal{E}_0(k) \sim H(k - 212) - H(k - 812)$  centered on  $k_0 = 512$  and constant for  $k \in [212, 812]$ .

The simulation parameters are listed in Table I. In column 7 we give an effective initial Reynolds number  $\text{Re}(0) = [N_{\text{eff}}/k_E(0)]^2$ , where  $k_E(0)$  is the initial energy centroid wave number. For the PS simulations  $N_{\text{eff}} = k_{\text{max}}$ , where  $k_{\text{max}} = 3072$  is the maximum resolved wave number, since dealiasing is achieved with a spectral filter [22].

To allow comparison between simulations, we define a dimensionless time

$$\tau = t/T_\omega, \quad (8)$$

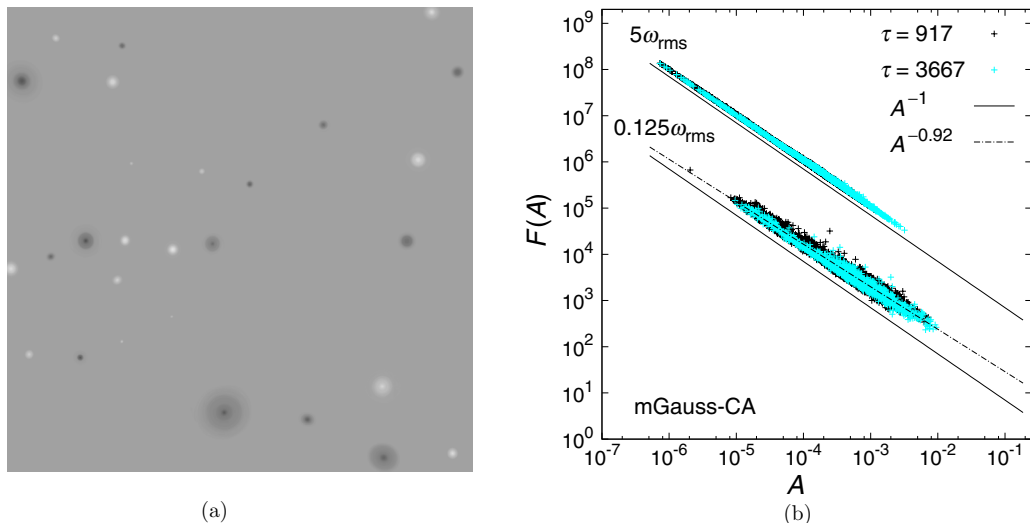


FIG. 1. (a) Coherent vortices on a  $4096^2$  subdomain from simulation mGauss-CA at  $\tau = 3667$  as selected by  $\omega_{\text{thr}} = 0.125\omega_{\text{rms}}$  and (b)  $F(A)$  as defined in Eq. (9) for two thresholds at the indicated times, with best fit line for  $\omega_{\text{thr}} = 0.125\omega_{\text{rms}}$  and  $A^{-1}$  scaling for comparison.

where  $T_\omega = 4\pi/\omega_{\text{rms}}(0)$  is an eddy turnover time and  $\omega_{\text{rms}}(0)$  is the rms vorticity of the initial vorticity field.

### III. VORTEX IDENTIFICATION

For most analyses, vortices are identified by finding all structures that exceed a given vorticity magnitude threshold and have an eccentricity  $e = \sqrt{1 - \lambda_2/\lambda_1}$  below a specified value, chosen to be  $e = 0.85$  after carefully examining the resulting coherent fields. Here  $\lambda_1$  and  $\lambda_2$  are the eigenvalues of the covariance matrix formed from the second-order moments of  $\omega$ , and  $\mathcal{D}_v$  is a subdomain restricted to the vortex in question. The eccentricity criterion has the greatest effect at early times, when mergers are more frequent and vortices tend to be more distorted. In addition, the peak vorticity magnitude within the region is required to exceed a tertiary threshold  $\omega_{\text{thr}}^{\text{ext}}$ . This ensures that the vortices are in fact concentrated regions of intense vorticity. Unless otherwise stated, the extraction parameters are  $\omega_{\text{thr}} = 0.125\omega_{\text{rms}}$  (mGauss-CA) and  $\omega_{\text{thr}} = \omega_{\text{rms}}$  (Gauss-PS, Tophat-CA, Tophat-PS),  $\omega_{\text{thr}}^{\text{ext}} = 2\omega_{\text{rms}}$ , and  $e = 0.85$ . Figure 1(a) shows coherent vortices from simulation mGauss-CA at  $\tau = 3667$  on a  $4096^2$  subdomain for  $\omega_{\text{thr}} = 0.125\omega_{\text{rms}}$ ,  $e = 0.85$ , and  $\omega_{\text{thr}}^{\text{ext}} = 2\omega_{\text{rms}}$ .

To check whether the vortex profiles are self-similar we follow [3] and postulate a similarity form  $\omega_v = \bar{\omega}_v f(r/R_v)$ , where  $\bar{\omega}_v$  is the vorticity averaged over the specific vortex of radius  $R_v$  and  $f$  is a universal dimensionless function. If the vortex profile is independent of spatial scale, then

$$F(A) \equiv \left( \int_0^{R_v} \omega \, dx \, dy \right)^{-2} \int_0^{R_v} \omega^2 \, dx \, dy \quad (9)$$

should scale like  $A^{-1} \sim R_v^{-2}$ [3]. In fact, this holds to a very good degree, provided  $\omega_{\text{thr}}$  is taken large enough, as shown in Fig. 1(b) for simulation mGauss-CA. There is a weak dependence of the best fit line on  $\omega_{\text{thr}}$ , with  $F(A) \sim A^{-0.92}$  for  $\omega_{\text{thr}} = 0.125\omega_{\text{rms}}$ ,  $F(A) \sim A^{-0.97}$  for  $\omega_{\text{thr}} = \omega_{\text{rms}}$  (not shown), and  $F(A) \sim A^{-0.98}$  for  $\omega_{\text{thr}} = 5\omega_{\text{rms}}$ .

The point scatter decreases as  $\omega_{\text{thr}}$  increases; this is because higher thresholds select the vortex cores and omit the undulating skirts acquired through merger, which depend on the history of the particular vortex and are less universal. The findings are similar for all other simulations independent

of initial condition and support universal  $A$ -independent profiles for the vortex cores, but less so the skirts, which are found preferentially on stronger and larger vortices.

#### IV. SCALING

We consider raw and compensated number densities in the forms

$$n(A,t) = c(t)A^{-r} \sim t^{-\alpha} A^{-r}, \quad (10)$$

$$n(A,t)/\overline{\omega_v^2}(A,t) = \tilde{c}(t)A^{-\tilde{r}} \sim t^{-\tilde{\alpha}} A^{-\tilde{r}}, \quad (11)$$

where tildes distinguish the exponents of the extended scaling form (11) from the exponents of the raw density (10). We will measure the exponents over appropriate ranges in the simulations listed in Table I. In Sec. IV A we examine the scaling in area ( $r$  and  $\tilde{r}$ ) and in Sec. IV B the scaling in time ( $\alpha$  and  $\tilde{\alpha}$ ).

##### A. Scaling in area $A$

Vortex number densities  $n(A,t)$ , intensities  $\overline{\omega_v^2}(A,t)$ , and vortex peak vorticities  $\overline{\omega^{\text{ext}}}$  are shown in Fig. 2 for the simulations mGauss-CA (top row) and Gauss-PS (bottom row) initialized with Gaussian energy spectra. In all panels cyan and pink symbols correspond to instantaneous values, while open black symbols represent time averages. The number densities are normalized by the total number of vortices  $N_v(t)$ : This collapses the densities, which can then be time averaged without knowing their decay rate, separating the  $A$  dependence from time evolution and allowing the scaling exponents  $\tilde{\alpha}$  and  $\tilde{r}$  to be measured independently.

The vortex intensity  $\overline{\omega_v^2}(A,t)$  is displayed in Figs. 2(a) and 2(c), where the black open triangles correspond to a time average and the pink diamonds to instantaneous values. As is evident,  $\overline{\omega_v^2}(A,t)$  varies significantly with  $A$  and the number density noticeably departs from  $A^{-1}$  scaling, with a break in the scaling located at the vortex area  $A_p$  where the vortex intensity distribution  $\overline{\omega_v^2}(A,t)$  reaches its maximum. This is true in both simulations, though the shape of the number density differs at  $A < A_p$ : In mGauss-CA  $n(A,t)$  is roughly flat at these scales, while in Gauss-PS it increases steeply with  $A$ .

In simulation mGauss-CA there is a systematic depletion in time of  $\overline{\omega_v^2}(A,t)$  in the smaller-scale range left of  $A_p$  in Fig. 2(a); this is consistent with a corresponding falloff in the average amplitude  $\overline{\omega^{\text{ext}}}$  of the vortex peaks at smaller scales and its relative constancy at larger scales in Fig. 2(b) (open black triangles and pink diamonds). The nonuniform distribution and evolution of  $\overline{\omega^{\text{ext}}}$  most likely reflect the spectrum of peaks in the initial vorticity field combined with a tendency for stronger vortices to survive merger more frequently. Weaker vortices are more likely to be strained out and destroyed or wrapped around larger vortices. The smaller-scale range left of  $A_p$  may be preferentially depleted through vortex destruction during interactions with larger vortices, which in contrast undergo lossless mergers, preserving  $\overline{\omega_v^2}(A,t)$ , as shown in the range to the right of  $A_p$ .

In Figs. 2(b) and 2(d) we show that the combination  $N_v^{-1}n(A,t)/\overline{\omega_v^2}(A,t)$  yields a range with approximate  $A^{-1}$  scaling in both simulations. A least-squares fit gives slopes of  $-1.02 \pm 0.04$  and  $-0.98 \pm 0.03$ , respectively, where the error is the standard deviation from the mean slope. The ranges over which the fits are obtained are indicated by the lines in Figs. 2(b) and 2(d). Note that the spread in the compensated density  $N_v^{-1}n(A,t)/\overline{\omega_v^2}(A,t)$  in simulation mGauss-CA [Fig. 2(b)], especially at small scales, is random in time: There is no systematic decay or growth, which justifies the extension of the fit line to these small scales.

We next consider the simulations initialized with top-hat energy spectra: Number densities  $n(A,t)$ , vortex intensities  $\overline{\omega_v^2}(A,t)$ , and vortex peak vorticities  $\overline{\omega^{\text{ext}}}$  are shown in Fig. 3 for simulation Tophat-CA (top row) and Tophat-PS (bottom row). Again, open black symbols represent time

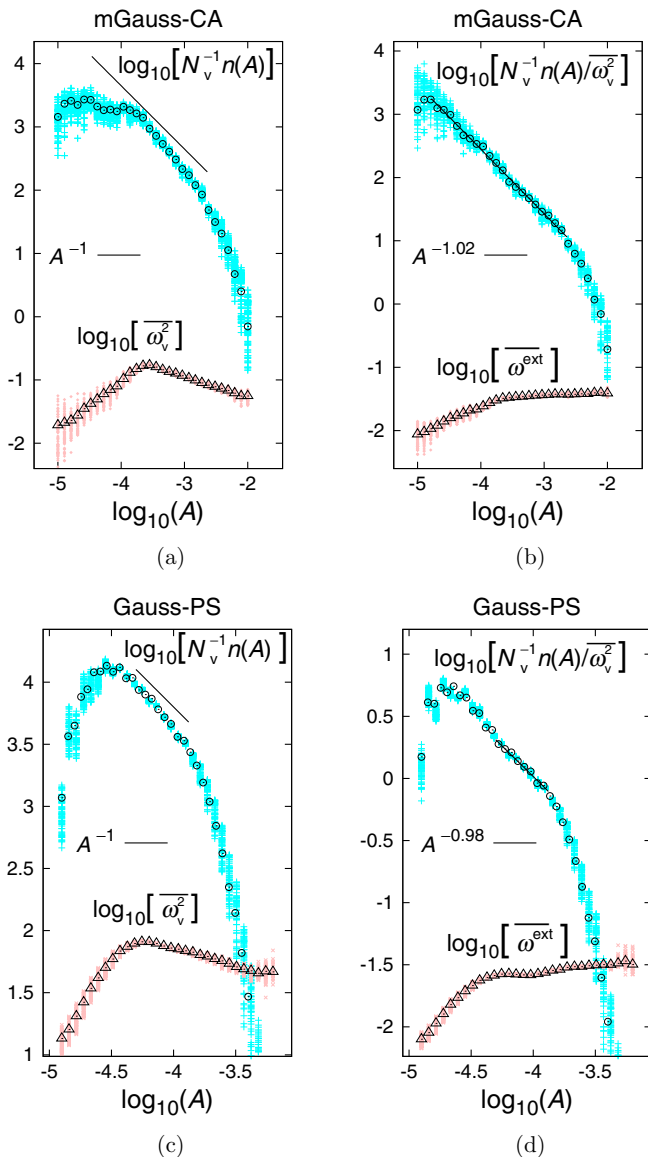


FIG. 2. (a) mGauss-CA and (c) Gauss-PS intensities  $\overline{\omega_v^2}$  and normalized number densities  $N_v^{-1}n(A,t)$ , where  $N_v(t)$  is the total number of vortices, for  $\omega_{\text{thr}} = 0.125\omega_{\text{rms}}$  (mGauss-CA) and  $\omega_{\text{thr}} = \omega_{\text{rms}}$  (Gauss-PS). (b) mGauss-CA and (d) Gauss-PS vortex peak vorticities  $\overline{\omega^{\text{ext}}}$  and compensated number densities  $N_v^{-1}n(A)/\overline{\omega_v^2}$ , with best fit lines  $A^{-1.02}$  and  $A^{-0.98}$ ; here  $\tilde{r} = 1.02 \pm 0.04$  (mGauss-CA) and  $\tilde{r} = 0.98 \pm 0.03$  (Gauss-PS), where the error is the standard deviation. Cyan and pink symbols are instantaneous and open black symbols are time-averaged values.

averages, while pink and cyan symbols are instantaneous values. The vortex intensity  $\overline{\omega_v^2}(A,t)$  varies much more weakly with  $A$  in these simulations, as shown in Figs. 3(a) and 3(c) (open black triangles and pink diamonds). In both simulations there is an approximate  $A^{-1}$  scaling range in the number density  $n(A,t)$  coinciding with a range of scales over which  $\overline{\omega_v^2}(A,t)$  is approximately constant. In simulation Tophat-CA the scaling exponent in the range  $[-3.54, -2.39]$  is  $r = 1.03 \pm 0.05$ , as

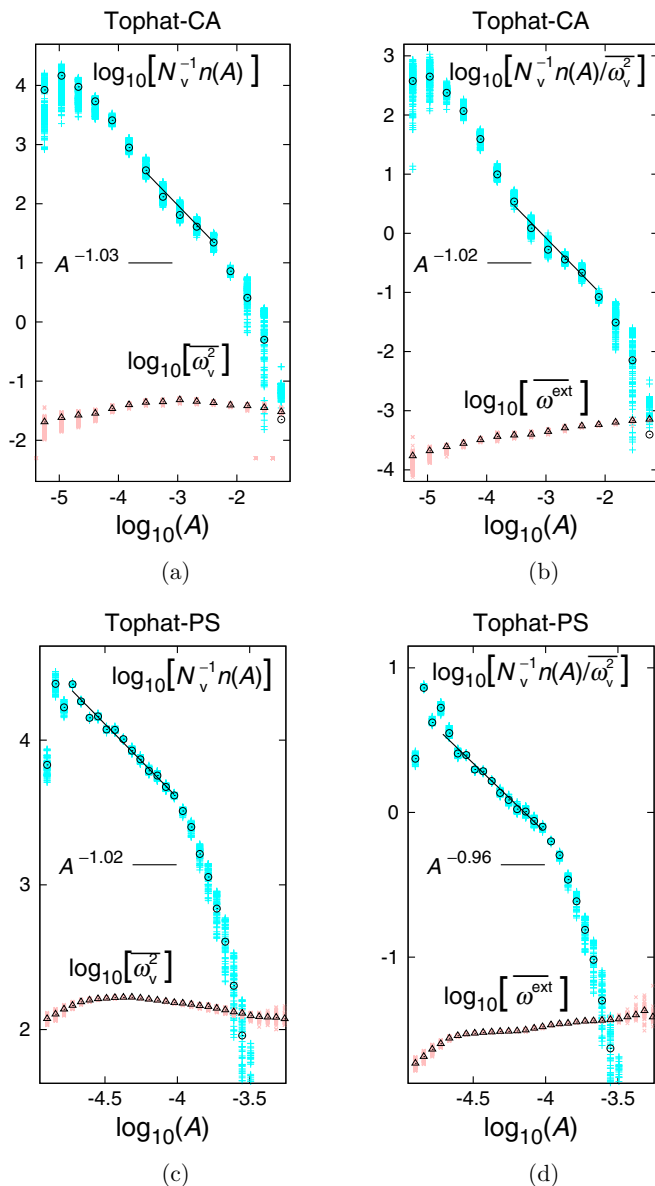


FIG. 3. (a) Tophat-CA and (c) Tophat-PS intensities  $\overline{\omega_v^2}(A, t)$  and normalized number densities  $N_v^{-1}n(A, t)$ , where  $N_v(t)$  is the total number of vortices, for  $\omega_{\text{thr}} = \omega_{\text{rms}}$ . (b) Tophat-CA and (d) Tophat-PS compensated number densities  $N_v^{-1}n(A, t)/\overline{\omega_v^2}(A, t)$  and vortex peak vorticities  $\overline{\omega^{\text{ext}}}$ . Cyan and pink symbols are instantaneous values, while open black symbols are time-averaged values. The error bars on the scaling exponents  $r$  and  $\tilde{r}$  can be found in Table III.

shown in Fig. 3(a) (solid black line). In simulation Tophat-PS a fit over the range  $[-4.72, -4.02]$  yields  $r = 1.02 \pm 0.02$ , as shown in Fig. 3(c) (solid line). Compensating the density by  $\overline{\omega_v^2}(A, t)$  yields an extended  $A^{-1}$  scaling range at  $A > A_p$  in simulation Tophat-CA, as indicated by the solid black fit line over the range  $[-3.54, -2.11]$  where the exponent is  $\tilde{r} = 1.02 \pm 0.05$ . The compensated density in simulation Tophat-PS has an exponent  $\tilde{r} = 0.96 \pm 0.06$  in the range  $[-4.72, -4.02]$

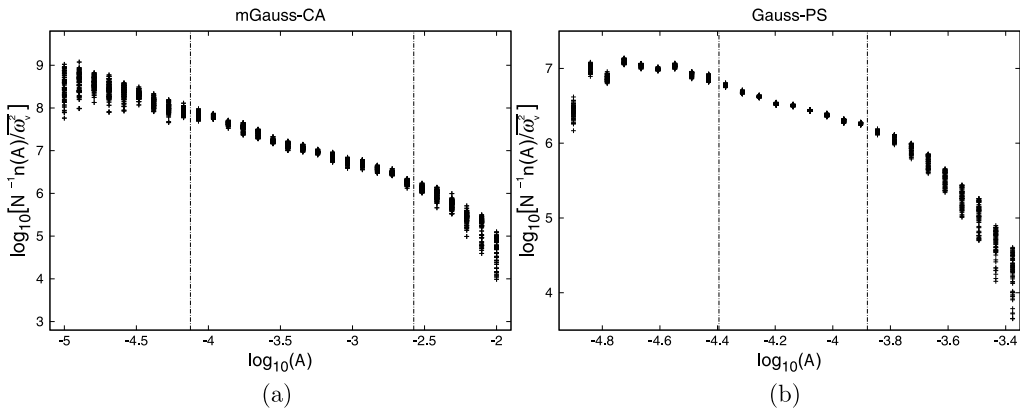


FIG. 4. Fit range used to compute the best-collapse temporal scaling exponent  $\tilde{\alpha}$  for simulations mGauss-CA (left) and Gauss-PS (right), illustrated for extractions with  $\omega_{\text{thr}} = 0.125\omega_{\text{rms}}$  (mGauss-CA) and  $\omega_{\text{thr}} = \omega_{\text{rms}}$  (Gauss-PS),  $e = 0.85$ , and  $\omega_{\text{thr}}^{\text{ext}} = 2\omega_{\text{rms}}$ . Points between the vertical dash-dotted lines are used in computing the values  $\tilde{\alpha} = 0.64 \pm 0.07$  (mGauss-CA, left) and  $\tilde{\alpha} = 0.65 \pm 0.06$  (Gauss-PS, right), which best collapse the number densities over these ranges.

indicated by the black fit line, so it also follows an  $A^{-1}$  scaling to within the error bars. We thus have the general result that compensating the number density by  $\overline{\omega_v^2}(A, t)$  yields an  $A^{-1}$  range.

### B. Temporal scaling

We now turn to measuring the overall temporal scaling exponents. To determine what factor of  $t$  best collapses the number densities, we consider pairs of densities at well separated times, compensating these by  $t^\alpha$  or  $t^{\tilde{\alpha}}$ , where the scaling exponent is varied from 0.5 to 0.8 in increments of 0.01. To determine the best-collapse exponent, we calculate the area in log-log space between the number density curves for each value of  $\alpha$  or  $\tilde{\alpha}$  considered. The value that minimizes the enclosed area is taken as the best-collapse temporal scaling exponent for that pair of times. To estimate an error in the exponents, this procedure is repeated for multiple pairs of times, the average best-collapse exponent is computed, and the error is the standard deviation about the mean. In selecting the range of scales over which to compute the area used to determine the degree of collapse, we must omit bins at small scales, where the occupation numbers fluctuate a great deal, as well as bins at large scales, which fill up in time. The selection of the fit range is illustrated in Fig. 4 for simulations mGauss-CA (left) and Gauss-PS (right): The bins between the vertical dashed lines are used to calculate the average best-collapse exponents of  $\tilde{\alpha} = 0.64 \pm 0.07$  (mGauss-CA, left) and  $\tilde{\alpha} = 0.65 \pm 0.04$  (Gauss-PS, right). As long as the noisy small scales and nonequibrated large scales are avoided, there is some leeway in selecting the bins: For example, if the bins on either side of the lines are included, or conversely if the fit range is shortened, the exponent is still  $\tilde{\alpha} = 0.66$  to within the error. Further, this result is insensitive to the vorticity threshold  $\omega_{\text{thr}}$ , as demonstrated in the Appendix.

### C. Scale invariance

We expect the extended self-similar form  $n(A, t)/\overline{\omega_v^2}(A, t) \sim t^{-2/3} A^{-1}$  to ensure some form of scale invariance in the vortex population. A natural vortex time scale is the turnover time  $T_v \equiv [\overline{\omega_v^2}(A, t)]^{-1/2}$ . We associate with this a dynamical length scale  $L_v$  defined as the distance over which a vortex of area  $A$  traveling at the mean speed  $\bar{u} \equiv \sqrt{2E}$ , where  $E$  is the energy defined in Eq. (3),

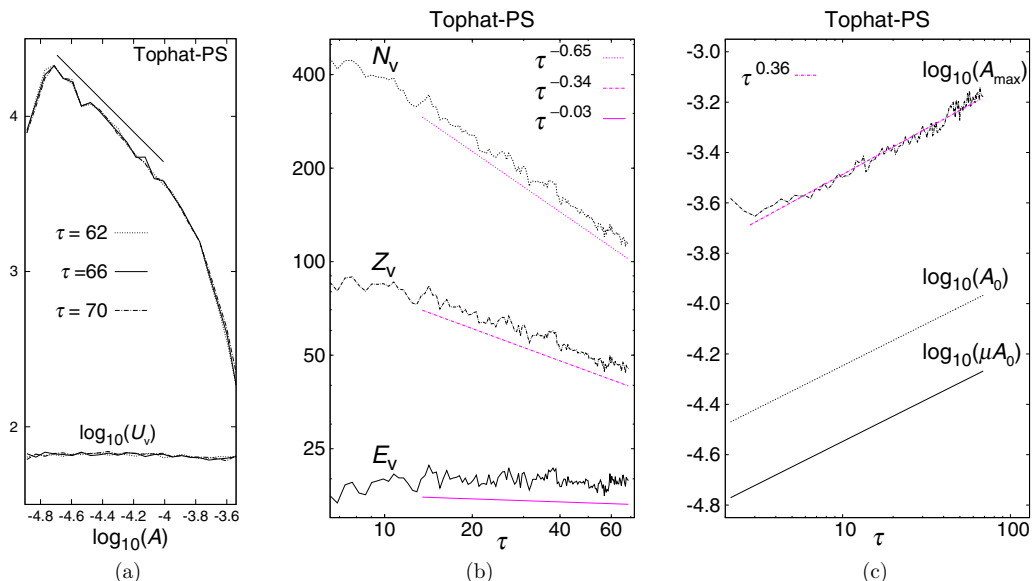


FIG. 5. (a) Tophat-PS number density  $n(A,t)$  and vortex translational speed  $U_v$  as functions of  $A$  at three times. Also shown are (b)  $N_v$  (dotted line),  $Z_v$  (dash-dotted line), and  $E_v$  (solid line) for the  $A^{-1}$  range. The scaling exponents are  $-0.65 \pm 0.01$ ,  $-0.34 \pm 0.01$ , and  $-0.03 \pm 0.01$ . (c) End points of the corresponding comoving interval  $[\mu A_0(\tau), A_0(\tau)]$  and area  $A_{\max}$  of the largest vortex. The scaling exponent for  $A_{\max}$  is  $0.36 \pm 0.03$ .

completes one turnover,

$$L_v(A,t) \equiv \bar{u} [\overline{\omega_v^2(A,t)}]^{-1/2}. \quad (12)$$

We assume that all vortices travel at the same mean speed  $\bar{u}$ , which holds very well, as shown for simulation Tophat-PS in Fig. 5(a), where the lower set of curves are the vortex translational speed  $U_v$  as a function of  $A$  at three times. The characteristic intervortex distance  $L_r(A,t)$  between vortices of a given scale  $A$  is

$$L_r(A,t) \equiv \left[ \frac{1}{D} \int_{\mu A}^A n(A',t) dA' \right]^{-1/2} \sim \sqrt{\frac{Dt^{2/3} \overline{\omega_{\max}^2}}{\overline{\omega_v^2(A,t)}}}, \quad (13)$$

where  $0 \ll \mu < 1$  is a constant, and we have inserted  $n(A,t) \sim t^{-2/3} \overline{\omega_v^2(A,t)} \omega_{\max}^{-2} A^{-1}$ , where  $\omega_{\max}$  is the conserved global vorticity maximum. Using this with (12) and assuming energy conservation, we obtain

$$\frac{L_r(A,t)}{L_v(A,t)} \sim t^{1/3}, \quad (14)$$

showing that the ratio of the characteristic intervortex distance to the distance traveled in one turnover time is independent of scale.

Figure 5(b) shows the evolution of the vortex number  $N_v = \int n(A,t) dA$ , vortex energy  $E_v$ , and vortex enstrophy  $Z_v$  in the Tophat-PS vortex population averaged over an ensemble of three simulations. Here and in the discussion of Fig. 6 we use the nondimensional time  $\tau$  in order to characterize the stage of flow evolution. The quantities  $N_v$ ,  $Z_v$ , and  $E_v$  are integrated over a comoving interval  $[\mu A_0(\tau), A_0(\tau)]$ , where  $A_0(\tau) \sim \tau^{1/3}$ , whose end points are shown in Fig. 5(c). For reference we also show the area  $A_{\max}$  of the largest vortex, again averaged over a three-member ensemble;  $A_{\max} \sim \tau^{0.36 \pm 0.03}$ , as determined by a least-squares best fit, where the error is the standard

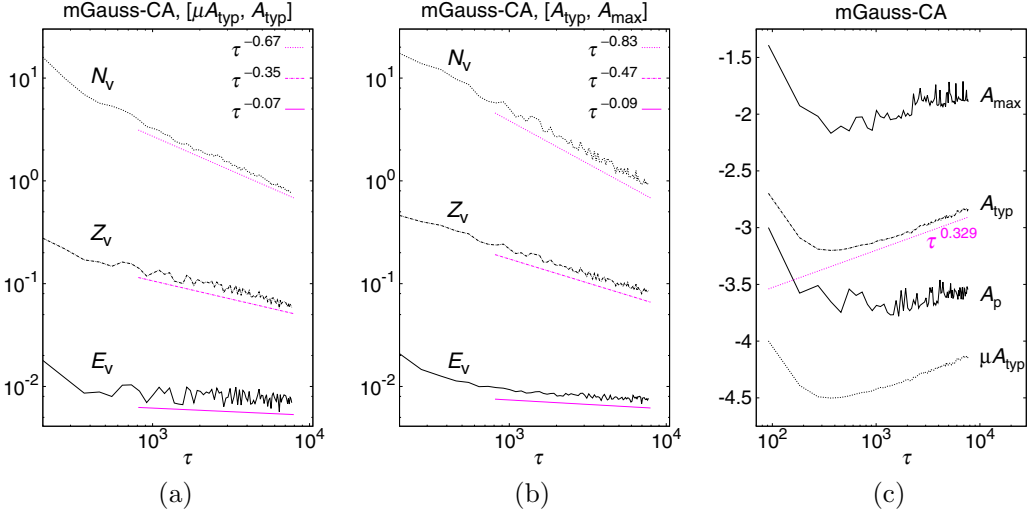


FIG. 6. Plot of  $N_v$  (dotted line),  $Z_v$  (dash-dotted line), and  $E_v$  (solid line) for (a) a comoving interval  $[\mu A_{\text{typ}}(\tau), A_{\text{typ}}(\tau)]$  and (b) a comoving interval  $[A_{\text{typ}}(\tau), A_{\text{max}}(\tau)]$ . The measured scaling exponents are (a)  $-0.67 \pm 0.01$ ,  $-0.35 \pm 0.03$ , and  $-0.07 \pm 0.05$  and (b)  $-0.83 \pm 0.02$ ,  $-0.47 \pm 0.01$ , and  $-0.09 \pm 0.01$ . (c) Interval end points  $\mu A_{\text{typ}}$ ,  $A_{\text{typ}}$ , and  $A_{\text{max}}$ , with  $A_p$  for reference and a fit line for comparison. The scaling exponent for  $A_{\text{typ}}$  is  $0.329 \pm 0.005$ .

deviation from the ensemble mean. A comparison of Figs. 5(a) and 5(c) shows that the end points fall within the range where  $n(A, t) \sim A^{-1}$ . The vortex number and enstrophy follow the scaling laws  $N_v \sim \tau^{-2/3}$  and  $Z_v \sim \tau^{-1/3}$  to within the estimated error, consistent with the number density (5) and vortex area growth law  $A(\tau) \sim \tau^{1/3}$  following from the scale-invariant theory of [7]; there is a slight decay in  $E_v$ . The measured decay laws, as shown in magenta in Fig. 5(b), are  $N_v \sim \tau^{-0.65 \pm 0.01}$ ,  $Z_v \sim \tau^{-0.34 \pm 0.01}$ , and  $E_v \sim \tau^{-0.03 \pm 0.01}$ .

The conservation properties of the mGauss-CA number density are shown in Fig. 6. In Fig. 6(a)  $N_v$ ,  $Z_v$ , and  $E_v$  are shown integrated over a comoving interval  $[\mu A_{\text{typ}}(\tau), A_{\text{typ}}(\tau)]$ , where

$$A_{\text{typ}}(\tau) \equiv \frac{1}{2} \frac{\int_{A_{\text{min}}}^{A_{\text{max}}} \overline{\omega_v^2}(A, t) A^2 n(A, t) dA}{\int_{A_{\text{min}}}^{A_{\text{max}}} \overline{\omega_v^2}(A, t) A n(A, t) dA} \quad (15)$$

is an intensity-weighted typical vortex area. As shown in Fig. 6(c),  $A_{\text{typ}} \sim \tau^{0.329 \pm 0.005}$ , where the error is the asymptotic standard error of the least-squares fit. Identifying the total energy with the vortex energy  $E \sim E_v$ , we note that  $A_{\text{typ}}$  corresponds to the vortex area  $l_\omega^2 \sim E/Z$  defined by Eq. (2.3) of [8]. The corresponding characteristic wave number  $k_\omega \sim \sqrt{Z/E}$  has appeared previously in [23], where its relationship to the minimum and maximum wave numbers in the system determines the equilibrium regime of the flow.

Despite the lack of scale invariance in the raw number density, the subpopulation of vortices contained in  $[\mu A_{\text{typ}}(\tau), A_{\text{typ}}(\tau)]$  approximately follows the decay laws  $N_v \sim \tau^{-2/3}$ ,  $Z_v \sim \tau^{-1/3}$ , and  $E_v \sim \tau^0$  predicted by the scale-invariant theory of [7]; the measured decay laws are  $N_v \sim \tau^{-0.67 \pm 0.01}$ ,  $Z_v \sim \tau^{-0.35 \pm 0.03}$ , and  $E_v \sim \tau^{-0.07 \pm 0.05}$ , as shown in magenta in Fig. 6(a). In contrast, as shown in Fig. 6(b), the vortex enstrophy decay rate in the comoving interval  $[A_{\text{typ}}(\tau), A_{\text{max}}(\tau)]$  is  $Z_v \sim \tau^{-0.47 \pm 0.01}$ , which is approximately the decay rate of the total enstrophy, suggesting that vortex interactions in this range of scales are predominantly responsible for the overall enstrophy decay.

## V. CONCLUSION

The scaling of vortices in decaying two-dimensional turbulence is found to be sensitive to initial conditions. Flows initialized with Gaussian energy spectra develop vortex intensity distributions  $\overline{\omega_v^2}(A, t)$  that are nonuniform in  $A$  and time evolving. Top-hat initial spectra, in contrast, yield vortex intensities that depend more weakly on vortex area and time.

When  $\overline{\omega_v^2}(A, t)$  varies significantly with  $A$  and  $t$ , scale invariance in the vortex area distribution is lost, but is recovered when the number density is compensated by  $\overline{\omega_v^2}(A, t)$ , giving the self-similar form  $n(A, t)/\overline{\omega_v^2}(A, t) \sim t^{-2/3} A^{-1}$ . This form ensures that the number of turnaround times  $[\overline{\omega_v^2}(A, t)]^{-1/2}$  taken to cross the average intervortex distance is independent of scale, which is a basic requirement for self-similar vortex dynamics. In this case, two scaling ranges appear in  $\overline{\omega_v^2}(A, t)$  and  $n(A, t)$ : In the small-scale range, which on average contains weaker vortices,  $\overline{\omega_v^2}(A, t)$  is depleted in time, while in the large-scale range, where vortices are stronger,  $\overline{\omega_v^2}(A, t)$  is constant. This reflects the tendency of larger, stronger vortices to survive mergers, while smaller, weaker vortices are absorbed or strained out and rendered passive. Hence, vortex interactions tend to enhance an initially nonuniform vorticity distribution. On the other hand, when the vortex intensity  $\overline{\omega_v^2}(A, t)$  does not vary appreciably with  $A$  or in time, the predictions of [7] hold in a scale-invariant range in which  $n(A, t) \sim t^{-2/3} A^{-1}$ . This solution, which is associated with a scale-invariant distribution of vortex areas, thus appears as a special case for initial conditions having  $\overline{\omega_v^2}(A, t)$  sufficiently uniform in  $A$  and  $t$ .

Finally, we have extended the concept of conservation in comoving intervals introduced in [8] to study the conservation properties of the scaling ranges. In simulations where  $\overline{\omega_v^2}(A, t)$  is uniform in  $A$  and constant in time, vortex energy  $E_v$  is conserved in a comoving interval  $[\mu A(t), A(t)]$ , where  $A(t) \sim t^{1/3}$ , as long as the end points fall within the range where  $n(A, t) \sim A^{-1}$ . Vortex number and vortex enstrophy satisfy  $N_v \sim t^{-2/3}$  and  $Z_v \sim t^{-1/3}$ , respectively, consistent with  $n(A, t) \sim t^{-2/3} A^{-1}$ .

TABLE II. Sensitivity of the compensated number density  $n(A, t)/\overline{\omega_v^2}(A, t) \sim t^{-\tilde{\alpha}} A^{-\tilde{r}}$  to vorticity threshold  $\omega_{\text{thr}}$ , with  $e = 0.85$  and  $\omega_{\text{thr}}^{\text{ext}} = 2\omega_{\text{rms}}$ , respectively. The ranges in  $\log_{10}(A)$  used to determine  $\tilde{r}$  and  $\tilde{\alpha}$  are given in columns 3 and 5, respectively. The scaling exponent  $\tilde{r}$  found by a least-squares fit is given in column 4 and the best-collapse temporal scaling exponent  $\tilde{\alpha}$  is given in column 6. Errors are estimated as the standard deviation.

Simulation	$\omega_{\text{thr}}$	Fit range, $\tilde{r}$	$\tilde{r}$	Fit range, $\tilde{\alpha}$	$\tilde{\alpha}$
mGauss-CA	$0.125\omega_{\text{rms}}$	$[-4.80, -2.62]$	$1.02 \pm 0.04$	$[-4.07, -2.62]$	$0.64 \pm 0.07$
mGauss-CA	$0.25\omega_{\text{rms}}$	$[-4.80, -2.62]$	$1.02 \pm 0.04$	$[-4.07, -2.62]$	$0.66 \pm 0.07$
mGauss-CA	$\omega_{\text{rms}}$	$[-5.10, -2.79]$	$1.00 \pm 0.03$	$[-3.97, -2.89]$	$0.67 \pm 0.07$
mGauss-CA	$2\omega_{\text{rms}}$	$[-5.20, -2.81]$	$0.96 \pm 0.03$	$[-4.16, -3.23]$	$0.64 \pm 0.07$
Gauss-PS	$0.5\omega_{\text{rms}}$	$[-4.26, -3.76]$	$0.97 \pm 0.05$	$[-4.26, -3.76]$	$0.63 \pm 0.07$
Gauss-PS	$\omega_{\text{rms}}$	$[-4.31, -3.90]$	$0.98 \pm 0.03$	$[-4.37, -3.90]$	$0.65 \pm 0.06$
Gauss-PS	$1.5\omega_{\text{rms}}$	$[-4.76, -4.18]$	$0.98 \pm 0.02$	$[-4.47, -4.18]$	$0.65 \pm 0.07$
Gauss-PS	$2\omega_{\text{rms}}$	$[-4.73, -4.11]$	$0.99 \pm 0.02$	$[-4.40, -4.20]$	$0.66 \pm 0.07$
Tophat-CA	$0.5\omega_{\text{rms}}$	$[-3.29, -1.85]$	$1.01 \pm 0.07$	$[-4.14, -1.85]$	$0.65 \pm 0.03$
Tophat-CA	$\omega_{\text{rms}}$	$[-3.54, -2.11]$	$1.02 \pm 0.05$	$[-4.39, -2.11]$	$0.67 \pm 0.08$
Tophat-CA	$1.5\omega_{\text{rms}}$	$[-3.59, -2.15]$	$1.03 \pm 0.03$	$[-4.44, -2.15]$	$0.63 \pm 0.08$
Tophat-CA	$2\omega_{\text{rms}}$	$[-3.69, -2.25]$	$0.95 \pm 0.05$	$[-4.54, -2.25]$	$0.65 \pm 0.07$
Tophat-PS	$0.5\omega_{\text{rms}}$	$[-4.51, -3.98]$	$0.94 \pm 0.07$	$[-4.51, -3.98]$	$0.65 \pm 0.06$
Tophat-PS	$\omega_{\text{rms}}$	$[-4.72, -4.02]$	$0.96 \pm 0.07$	$[-4.72, -4.02]$	$0.60 \pm 0.7$
Tophat-PS	$1.5\omega_{\text{rms}}$	$[-4.80, -4.07]$	$1.01 \pm 0.06$	$[-4.80, -4.07]$	$0.61 \pm 0.07$
Tophat-PS	$2\omega_{\text{rms}}$	$[-4.81, -4.11]$	$0.98 \pm 0.03$	$[-4.81, -4.18]$	$0.64 \pm 0.06$

TABLE III. Sensitivity of the raw number density  $n(A, t) \sim t^{-\alpha} A^{-r}$  to vorticity threshold  $\omega_{\text{thr}}$  in simulations Tophat-CA and Tophat-PS, with  $e = 0.85$  and  $\omega_{\text{thr}}^{\text{ext}} = 2\omega_{\text{rms}}$ . The ranges in  $\log_{10}(A)$  used to determine  $r$  and  $\alpha$  are given in columns 3 and 5, respectively. The scaling exponent  $r$  found by a least-squares fit is given in column 4 and the best-collapse temporal scaling exponent  $\alpha$  is given in column 6. Errors are estimated as the standard deviation.

Run	$\omega_{\text{thr}}$	Fit range, $r$	$r$	Fit range, $\alpha$	$\alpha$
Tophat-CA	$0.5\omega_{\text{rms}}$	$[-3.29, -2.14]$	$1.03 \pm 0.07$	$[-4.14, -1.85]$	$0.64 \pm 0.03$
Tophat-CA	$\omega_{\text{rms}}$	$[-3.54, -2.39]$	$1.03 \pm 0.05$	$[-4.39, -2.11]$	$0.66 \pm 0.03$
Tophat-CA	$1.5\omega_{\text{rms}}$	$[-3.59, -2.44]$	$1.03 \pm 0.05$	$[-4.44, -2.15]$	$0.65 \pm 0.03$
Tophat-CA	$2\omega_{\text{rms}}$	$[-3.69, -2.54]$	$1.06 \pm 0.05$	$[-4.54, -2.25]$	$0.66 \pm 0.03$
Tophat-PS	$0.5\omega_{\text{rms}}$	$[-4.51, -3.98]$	$1.03 \pm 0.03$	$[-4.51, -3.98]$	$0.59 \pm 0.08$
Tophat-PS	$\omega_{\text{rms}}$	$[-4.72, -4.02]$	$1.02 \pm 0.02$	$[-4.72, -4.02]$	$0.64 \pm 0.06$
Tophat-PS	$1.5\omega_{\text{rms}}$	$[-4.80, -4.07]$	$0.98 \pm 0.02$	$[-4.80, -4.07]$	$0.67 \pm 0.07$
Tophat-PS	$2\omega_{\text{rms}}$	$[-4.81, -4.18]$	$0.98 \pm 0.01$	$[-4.81, -4.18]$	$0.71 \pm 0.08$

When  $\overline{\omega_v^2}(A, t)$  varies significantly with  $A$  and  $t$  these decay rates still hold, but for a specific comoving interval  $[\mu A_{\text{typ}}(t), A_{\text{typ}}(t)]$ , where  $A_{\text{typ}} \sim t^{1/3}$  is a typical intensity-weighted vortex area.

In conclusion, our results demonstrate the existence of an extended form of scale invariance in the vortices of decaying two-dimensional turbulence. This result is yet more evidence that coherent vortex populations in two-dimensional turbulence exhibit nontrivial scaling properties, which extend beyond the classical similarity theories of Kraichnan and Batchelor. The discovery of these scaling properties represents a step toward a more complete description of two-dimensional turbulence.

#### APPENDIX: VORTICITY THRESHOLD SENSITIVITY

To establish the robustness of the number density to the vorticity threshold  $\omega_{\text{thr}}$  used to identify vortices, we computed scaling exponents for a range of thresholds in each simulation. Beginning with the extended scaling form (11), Table II shows the sensitivity of the scaling exponents  $\tilde{\alpha}$  and  $\tilde{r}$  of the compensated number density  $n(A, t)/\overline{\omega_v^2}(A, t) \sim t^{-\tilde{\alpha}} A^{-\tilde{r}}$  to  $\omega_{\text{thr}}$ . The name of the simulation is given in column 1, the value of  $\omega_{\text{thr}}$  in column 2, the fit range in  $\log_{10}(A)$  in column 3, and value of  $\tilde{r}$  obtained by a least-squares best fit in column 4. The error estimated in  $\tilde{r}$  is the standard deviation about the time-mean value of the exponent. Column 3 shows that  $\tilde{r} = 1$  and  $\tilde{\alpha} = 2/3$  to within the error bars for almost all values of  $\omega_{\text{thr}}$  considered, demonstrating the insensitivity of the extended scaling range to the vorticity threshold, as long as it is not taken so high that large numbers of vortices are excluded from the statistics. As a rule, the range over which the scaling holds moves to smaller scales as  $\omega_{\text{thr}}$  increases because the vortices become smaller.

Turning now to the uncompensated density equation (10), the sensitivity of the scaling exponents  $\alpha$  and  $r$  to the vorticity threshold in simulations Tophat-CA and Tophat-PS is explored in Table III. Again, for almost all values of  $\omega_{\text{thr}}$  the exponents are  $\alpha = 2/3$  and  $r = 1$  to within the error bars, demonstrating insensitivity of the number density scaling exponents to the vorticity threshold used to identify vortices.

- 
- [1] S. R. Green, F. Carrasco, and L. Lehner, A Holographic Path to the Turbulent Side of Gravity, *Phys. Rev. X* **4**, 011001 (2014).  
 [2] M. C. Tsatsos, P. E. S. Tavares, A. Cidrim, A. R. Fritsch, M. A. Caracanhas, F. E. A. dos Santos, C. F. Barenghi, and V. S. Bagnato, Quantum turbulence in trapped atomic Bose-Einstein condensates, *Phys. Rep.* **622**, 1 (2016).

- [3] R. Benzi, S. Patarnello, and P. Santangelo, Self-similar coherent structures in two-dimensional decaying turbulence, *J. Phys. A* **21**, 1221 (1988).
- [4] R. Benzi, M. Collela, M. Briscolini, and P. Santangelo, A simple point vortex model for two-dimensional decaying turbulence, *Phys. Fluids. A* **4**, 1036 (1992).
- [5] G. F. Carnevale, J. C. McWilliams, Y. Pomeau, J. B. Weiss, and W. R. Young, Evolution of Vortex Statistics in Two-Dimensional Turbulence, *Phys. Rev. Lett.* **66**, 2735 (1991).
- [6] J. B. Weiss and J. C. McWilliams, Temporal scaling behavior of decaying two-dimensional turbulence, *Phys. Fluids* **5**, 608 (1993).
- [7] D. G. Dritschel, R. K. Scott, C. Macaskill, G. A. Gottwald, and C. V. Tran, Unifying Scaling Theory for Vortex Dynamics in Two-Dimensional Turbulence, *Phys. Rev. Lett.* **101**, 094501 (2008).
- [8] B. H. Burgess and R. K. Scott, Scaling theory for vortices in the two-dimensional inverse energy cascade, *J. Fluid Mech.* **811**, 742 (2017).
- [9] G. F. Carnevale, Y. Pomeau, and W. R. Young, Statistics of Ballistic Agglomeration, *Phys. Rev. Lett.* **64**, 2913 (1990).
- [10] G. Huber and P. Alstrom, Universal decay of vortex density in two dimensions, *Physica A* **195**, 448 (1993).
- [11] Y. Pomeau, Vortex dynamics in perfect fluids, *J. Plasma Phys.* **56**, 407 (1996).
- [12] E. Trizac and J.-P. Hansen, Dynamics and growth of particles undergoing ballistic coalescence, *J. Stat. Phys.* **82**, 1345 (1996).
- [13] T. Iwayama, H. Fujisaka, and H. Okamoto, Phenomenological determination of scaling exponents in two-dimensional decaying turbulence, *Prog. Theor. Phys.* **98**, 1219 (1997).
- [14] E. Trizac, A coalescence model for freely decaying two-dimensional turbulence, *Europhys. Lett.* **43**, 671 (1998).
- [15] C. Sire and P.-H. Chavanis, Numerical renormalization group of vortex aggregation in two-dimensional decaying turbulence, *Phys. Rev. E* **61**, 6644 (2000).
- [16] J. H. LaCasce, The vortex merger rate in freely decaying, two-dimensional turbulence, *Phys. Fluids* **20**, 085102 (2008).
- [17] M. Roos, *Introduction to Cosmology*, 4th ed. (Wiley, Chichester, 2015).
- [18] G. Haller, A. Hadjighasem, M. Farazmand, and F. Huhn, Defining coherent vortices objectively from the vorticity, *J. Fluid Mech.* **795**, 136 (2016).
- [19] N. J. Zabusky, Contour dynamics for the euler equations in two dimensions, *J. Comput. Phys.* **30**, 96 (1979).
- [20] M. A. Virasoro, Variational Principle for Two-Dimensional Incompressible Hydrodynamics and Quasi-geostrophic Flows, *Phys. Rev. Lett.* **47**, 1181 (1981).
- [21] D. G. Dritschel and J. Fontane, The combined Lagrangian advection method, *J. Comput. Phys.* **229**, 5408 (2010).
- [22] T. Y. Hou and R. Li, Dynamic depletion of vortex stretching and non-blowup of the 3-D incompressible euler equations, *J. Nonlinear Sci.* **16**, 639 (2006).
- [23] R. H. Kraichnan, Inertial ranges in two-dimensional turbulence, *Phys. Fluids* **10**, 1417 (1967).